Arabian Journal for Science and Engineering
https://doi.org/10.1007/s13369-020-05229-4

RESEARCH ARTICLE-CHEMISTRY

DFT and Electrochemical Investigations on the Corrosion Inhibition of Mild Steel by Novel Schiff's Base Derivatives in 1 M HCl Solution

S. Alaoui Mrani[1] · E. Ech-chihbi[1] · N. Arrousse[1] · Z. Rais[1] · F. El Hajjaji[1] · C. El Abiad[2] · S. Radi[2] · J. Mabrouki[3] · M. Taleb[1] · S. Jodeh[4]

Received: 8 May 2020 / Accepted: 9 December 2020

Abstract
This study aims to explore the inhibitory action of certain derivatives of Schiff's base, namely 4-(pyridin-2-ylimino) pentan-2-one (CE5),4-(pyrimidin-2-ylimino) pentan-2-one (CE4) and 4-((1H-tetrazol-5-yl) imino) pentan-2-one (CE20) against mild steel (MS) corrosion in 1 M HCl by the gravimetric, stationary and transient method. For additional information on the inhibitory properties of the studied compounds, scanning electron microscopy (SEM) and functional density theory (DFT) calculations were also performed. The effectiveness of the Schiff's base derivatives studied follows the order: CE20 > CE4 > CE5. The electrochemical impedance curves show that the corrosion reaction is controlled by a charge transfer process, while the potentiodynamic polarization curves indicate that the synthesized compounds act as a mixed-type inhibitor. The adsorption process follows the Langmuir isotherm. Kinetic, as well as thermodynamic parameters, were calculated and discussed. The increase in E_{HOMO} and decrease in gap energy ΔE_{gap} lead to an increase in the inhibition efficiency. Results obtained from quantum chemical studies are in good agreement with quantum chemical parameters and experimental inhibition efficiencies.

Keywords Schiff base derivatives · Electrochemical Impedance Spectroscopy · Scanning Electron Microscopy · Adsorption

1 Introduction

Mild steel has been recognized as a preferential material for several industrial and structural applications. It is generally used due to its relatively low cost and good mechanical properties [1]. Hydrochloric acid is commonly used in the pickling bath to remove impurities, such as stains, inorganic contaminants, rust or scale from ferrous metals. In addition, in this study we have chosen this concentration to get an idea of our inhibitors in environments which are very aggressive because the inhibitors which give a high efficiency in 1 M HCl automatically give remarkable results with low concentration of HCl [2, 3]. In spite of its required qualities, mild steel can be prone to corrosion while in contact with aggressive environments such as acidic media [4]. Among the various preventions adopted to increase the devastating effects and to control the rate of corrosion, one of the most effective methods is the employment of organic compounds. Corrosion inhibition by organic compounds is explained as the result of adsorption on the surface of the metal forming a protective layer; this layer blocks the active sites present on mild steel surface and thereby isolates the mild steel from corrosive attack [5].

Factors that mainly affect the adsorption mechanism of inhibitors to the metal surface are: the molecular structure, the nature of the metal, environment of metal–solution interface [6].

A compound's effectiveness in a chemical reaction is related to its geometric and electronic molecular structure. The geometry of the molecule is related to the optimal way in which the inhibitor might cover the metal surface then has a strong influence on the adsorbability of the inhibitor on the metal surface. Thus, compounds that have planar geometry

✉ S. Jodeh
sjodeh@hotmail.com

1 Engineering Laboratory of Organometallic, Molecular Materials and Environment, Faculty of Science, University Sidi Mohamed Ben Abdellah, P.O. Box 1796, Fez, Morocco

2 LCAE, Department of Chemistry, Faculty of Sciences, University Mohamed Premier, Oujda, Morocco

3 Laboratory of Materials, Nanotechnology and Environment, Department of Chemistry, Faculty of Sciences, Mohammed V University, Rabat, Morocco

4 Department of Chemistry, An-Najah National University, P.O. Box 7, Nablus, Palestine

Published online: 27 January 2021

often have higher inhibition efficiencies than corresponding compounds that have less planar geometry. Interactions between the inhibitor and the MS surface depend strongly on the electron density distribution in the inhibitors. Regions in the molecule with high electron densities would preferably donate electrons to partially filled or empty "*d*" orbitals of the metal resulting in a donor–acceptor binding [7].

Recently, Schiff base ligands (also known as imine) have shown a great inhibition efficiency in acidic media due to the presence of the –C=N– group; the nitrogen atom has unshared lone pair of electron which can form coordinate-covalent bonds with the metal surface by their unshared lone pairs of electrons, while the π-bond interacts physically to enhance their adsorption affinity [8–10]. DFT (Density functional theory) is a quantum mechanical calculation extensively employed to interpret experimental results and to obtain structural parameters for even huge complex molecules [11].

Accordingly, this study was undertaken to evaluate the adsorption behavior and inhibition effect of three newly synthesized Schiff base namely 4-(pyridin-2-ylimino) pentan-2-one, 4-(pyrimidin-2-ylimino) pentan-2-one and 4-((1H-tetrazol-5-yl) imino) pentan-2-one using Electrochemical Impedance Spectroscopy (EIS) and Potentiodynamic Polarization (PP) techniques. Furthermore, detailed DFT computations have been performed using a theoretical DFT method to establish the correlation between the inhibitor molecular structure and the inhibition impacts.

2 Materials and Methods

2.1 Inhibitors

See Table 1.

2.2 Synthesis

The ligand **CE4** was prepared according to the literature methods [12]. For **CE5** and **CE20**: a mixture of pentan-2,4-dione (25 mmol), 2-aminopyridine or 1*H*-tetrazol-5-amine (25 mmol) and ethanol (30 ml) was steered and heated at 75 °C for 16 h. The solution was cooled at room temperature to precipitate the product; the solid was filtered and washed with ethanol. The new ligands **CE5** and **CE20** were synthesized using a simple procedure by reacting an equimolar 1:1 of 2-aminopyridine or 1*H*-tetrazol-5-amine and pentan-2,4-dione. The desired products were isolated easily by precipitation in ethanol. Besides, **CE5** and **CE20** were characterized by ^{1}H, ^{13}C NMR and melting point (Scheme 1).

(2Z)-4-(pyridin-2-ylimino)pent-2-en-2-ol (CE5) Brown Solid. Yield: 60%. ^{1}H NMR (300 MHz, $DMSO_{d6}$) δ: 1.91 (s, 3H, CH_3–C–OH); 2.04 (s, 3H, CH_3–C=N), 5.25 (s, 1H, CH enol); 6.99 (m, 2H, H_{Py}); 7.06 (m, 1H, H_{Py}); 7.34 (m, 1H, H_{Py}).^{13}C NMR (300 MHz, $DMSO_{d6}$) δ: 20.08 (1C, C–C=N); 29.62 (1C,C–C–OH); 98.57 (1C,C=C), 119.51

Table 1 Molecular nomenclature, structures and abbreviated names of the exanimated inhibitors CE4, CE5 and CE20

Molecular name	Molecular structure	Abbreviations
(2Z)-4-(pyridin-2-ylimino)pent-2-en-2-ol	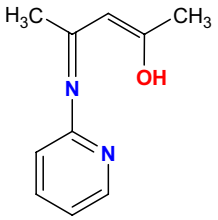	CE5
(2Z)-4-(pyrimidin-2-ylimino)pent-2-en-2-ol	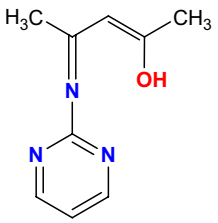	CE4
(2Z)-4-((1H-tetrazol-5-yl)imino)pent-2-en-2-ol	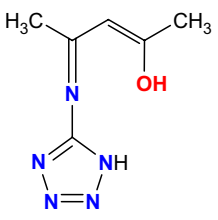	CE20

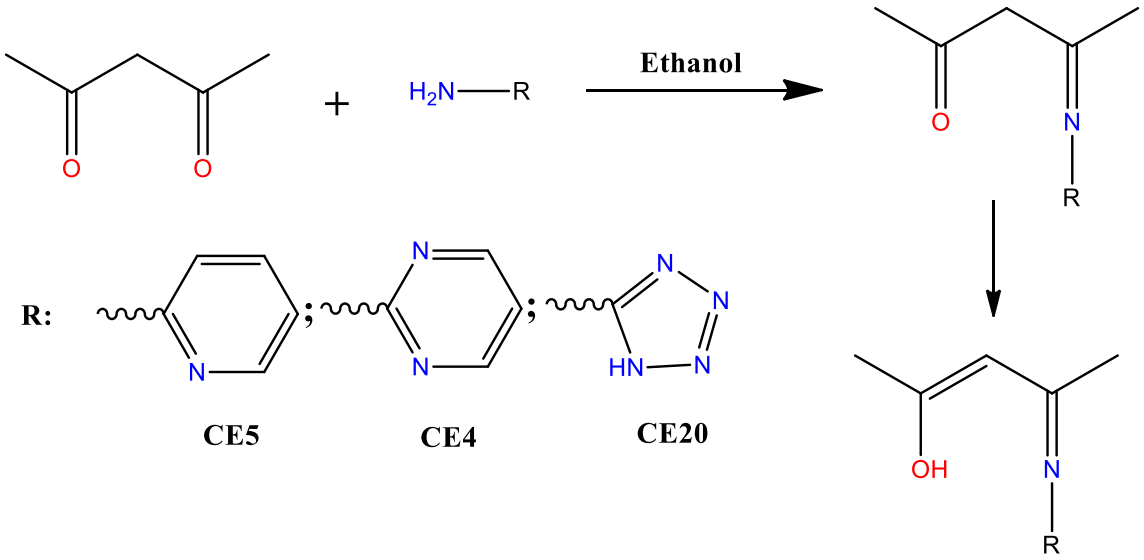

Scheme 1 Schematic preparation of the ligands **CE4**, **CE5,** and **CE20**

(1C, C_{Py}); 120.94 (1C, C_{Py}); 130.60 (1C, C_{Py}); 139.82 (1C, C_{Py}); 160.11 (2C, C_{Py} and C=N); 195.87 (1C,C–OH).Mp: 86–88 °C.

(2Z)-4-(pyrimidin-2-ylimino)pent-2-en-2-ol (CE4) Yellow Solid. Yield: 70%. ^{1}H NMR spectrum shows signals strong signals at δ 2.50 (3H, s), 3.44 (3H, s), 6.52–6.55 (1H, t), 6.62 (1H, s), 8.16–8.24 (2H, *d*) and 12.50 (1H, s) ppm. These have been assigned to –CH_3 protons, pyrimidine proton, pentan-2, 4-dione proton, pyrimidine protons and –OH proton. ^{13}C NMR spectrum shows signals at 40.02, 110.69, 158.58 and 164.13 ppm assigned to –CH_3 carbons, pentan-2, 4-dione carbons, pyrimidine carbons, and –C=N carbon.

(2Z)-4-((1H-tetrazol-5-yl)imino)pent-2-en-2-ol (CE20) White solid. Yield: 62%. ^{1}H NMR (300 MHz, $DMSO_{d6}$) δ: 2.67 (s, 3H, CH_3–C–OH); 2.86 (*d*, 3H, CH_3–C=N), 7.37 (m, 1H, CH enol).^{13}C NMR (300 MHz, $DMSO_{d6}$) δ: 16.94 (1C, C–C=N);25.46 (1C,C–C–OH); 113.75 (1C, C=C), 145.78 (1C, C_{Tz}); 155.15 (1C, C=N); 169.76 (1C, C–OH).Mp: 228–230 °C.

2.3 Mild Steel Specimens

For weight loss, electrochemical and SEM analyses, the mild steel composition is given as 0.38 wt% (Si), 0.21 wt% (C), 0.09 wt% (C), 0,05 wt% (S), 0,01 wt% (Al), 0,05 wt% (Mn) and 99.21 wt% (Fe) were employed. Before each test the specimens were polished with an abrasive paper (180–1200), rinsed by distilled H_2O, degreased with acetone and then dried under the flow of dry air.

2.4 Solutions

Analytical grade 37% HCl was diluted with distilled water to obtain the corrosive 1 M HCl solution. The range of concentration considered was 10^{-6} to 10^{-3}M of inhibitors.

2.5 Weight Loss Measurements

To evaluate the inhibition action of inhibitor, weight loss measurement was described in different literature publications. By using this method, the corrosion rate (ν) and inhibition efficiency ($EI_{\nu}\%$) were calculated from Eqs. (1) and (2), respectively, where m_0 and mi are the mass of the test specimen before and after corrosion, S is the specimen's surface, t is the immersion time, ν_i and ν_0 are corrosion rate of the MS specimen in HCl medium with and without different concentrations of inhibitors [13, 14]:

$$\nu_i = \frac{m_0 - m_i}{S.t} \tag{1}$$

$$\mathrm{EI}_{\nu}\% = \frac{\nu_0 - \nu_i}{\nu_0} \times 100. \tag{2}$$

2.6 Electrochemical Studies

The corrosion inhibition performance of CE4, CE5, and CE20 on MS in 1 M HCl was analyzed by standard electrochemical methods. A standard three-electrode cell assembly was constructed with 1 cm^2 exposed area of polished MS as working electrode (WE), saturated calomel electrode (Ag/AgCl) as reference electrode (RE) and platinum as counter

electrode (CE). The cell was connected to a PGZ 100 type Potentiostat controlled using the Volta master 4 software. All the experiments were performed after 30 min of immersion time to attain the equilibrium state. EIS study was obtained over a frequency range of 100 mHz to 100 kHz at OCP with alternating current ± 10 mV of amplitude. The Tafel studies were carried out by applying the electrode potential from − 800 to − 200 mV at a polarization scan rate of 1 mV s^{-1}. Both Tafel segments of cathodic and anodic curves were extrapolated to corrosion potential in order to determine the PP parameters.

The inhibition efficiency (IE_{PP}) was assessed by using i_{corr} values as given in Eq. (3) [15]:

$$IE_{PP}\% = \left[\frac{i_{corr} - i'_{icorr}}{i_{corr}}\right] \times 100 \quad (3)$$

where i_{corr} and i'_{corr} are the corrosion current without and with inhibitor, respectively.

2.7 SEM Analysis

The surface morphologies of MS specimen surface in the presence and absence of inhibitors were carried using SEM technique at low magnifications by using FEI quanta 200. For that, the samples were immersed in 1 M HCl alone and after addition of the effective inhibitor concentration for 6 h. After the immersion time, the test samples were drawn out and rinsed with distilled H_2O and finally dried to be analyzed.

2.8 DFT Computational Details

DFT calculations were accomplished using B3LYP at 6-31G (*d*, *p*) basis set for neutral and forms. All quantum calculations were performed for neutral forms in the gas phase using Gaussian 09 software package. The quantum chemical parameters extracted from the output file such as HOMO (highest occupied molecular orbit) and LUMO (lowest unoccupied molecular orbit), dipole moment (μ), softness (σ), fraction of electron transferred (ΔN), electrophilicity (ω), nucleophilicity (ε) and Fukui functions have been also calculated to understand the activity and corrosion inhibiting properties of the studied compounds.

2.9 Monte Carlo (MC) Simulation

This method was used to obtain the low configuration adsorption energy of the interactions of the three imines derivatives with iron surface in the presence of water. The COMPASS force field was used to optimize the structures of all components of the system. Then, we added 100 molecules of water to the simulation box and enlarged to (12 × 12) supercell with a vacuum slab of 50 Å. The Monte Carlo simulation was carried out using Adsorption Locator module in Materials Studio 7.0 software [16].

3 Results and Discussion

3.1 Weight Loss Measurements

Weight loss measurement is often exploited to determine the corrosion protection behavior of an inhibitor due to its simplicity. All weight loss measurements were repeated three times under the same conditions to obtain creditable values. The variation of the weight loss at 298 K is displayed in Table 2.

It appears from Table 2 that the rate of MS corrosion gradually decreases with the inhibitor's concentration. The inhibitory behavior of these compounds is allocated to their adsorption on the MS surface, which restricts the dissolution by blocking the corrosion sites which generates a corrosion rate decrease. The IEν (%) of the three inhibitors follows the order CE20 > CE4 > CE5 [15, 17].

3.2 Potentiodynamic Polarization Measurements

Potentiodynamic polarization is a suitable method for monitoring the progress and the mechanism of the anodic and the cathodic reactions as well as identifying the effect of inhibitor concentration on either cathodic or anodic reactions. Tafel curves for MS in the acidic solution with different

Table 2 Effect of concentration of imine derivatives in 1M HCl obtained from weight loss measurements at 298 K after 6 h of immersion

Medium	Concentration (M)	Corrosion rate (mg cm^{-2} h^{-1})	IE_ν (%)
1 M HCl	–	0.6532	–
CE4	10^{-3}	1.2280	***88***
	10^{-4}	1.2215	***87***
	10^{-5}	1.1104	***70***
	10^{-6}	0.7577	***16***
CE5	10^{-3}	1.1758	***80***
	10^{-4}	1.0517	***61***
	10^{-5}	0.9929	***52***
	10^{-6}	0.8688	***33***
CE20	10^{-3}	1.2411	***90***
	10^{-4}	1.2345	***89***
	10^{-5}	1.1431	***75***
	10^{-6}	0.8492	***30***

The values of the parameters marked in bolditalics are related to each other and have a significance on the protective power of the two products

concentrations of CE4, CE5, and CE20 are presented in Fig. 1.

Electrochemical corrosion kinetics parameters data obtained from the extrapolation of the polarization curves as a function of inhibitors concentrations, namely corrosion potential (E_{corr}), current density (i_{corr}), cathodic Tafel slopes (β_c) and inhibition efficiency (IE_{PP}) are displayed in Table 3.

From Fig. 1 and Table 3 it is obvious that the values of current density i_{corr} of MS after addition of the studied compounds are much smaller than that in the blank solution, which is explained by better adsorption of investigated molecules on the metal surface. These observations confirm that the studied compounds exhibit excellent inhibition performance against the corrosion of MS in the HCl solution [13]. The values of i_{corr} simultaneously decreased with inhibitor concentration and reached a minimum value at 10^{-3} M. Accordingly, IE_{PP} reaches a maximum value of 88% for CE20, indicating that this compound performs as an efficient inhibitor on MS corrosion in acidic solutions.

Table 3 Potentiodynamic polarization parameters for MS exposed to various corrosive solutions at 298 K

Medium	Concentration (M)	$-E_{corr}$ (mV/Ag/AgCl)	i_{corr} (µA cm^{-2})	$-\beta_c$ (mV dec^{-1})	IE_{PP} (%)
1 M HCl	–	436	***694***	139	–
CE4	10^{-3}	381	***98***	114	***86***
	10^{-4}	376	***114***	121	***84***
	10^{-5}	390	***232***	115	***67***
	10^{-6}	375	***604***	145	***13***
CE5	10^{-3}	387	***163***	112	***77***
	10^{-4}	379	***307***	141	***56***
	10^{-5}	389	***366***	168	***47***
	10^{-6}	376	***472***	146	***32***
CE20	10^{-3}	380	***84***	118	***88***
	10^{-4}	371	***92***	132	***87***
	10^{-5}	375	***193***	133	***72***
	10^{-6}	394	***514***	139	***26***

The values of the parameters marked in bolditalics are related to each other and have a significance on the protective power of the two products

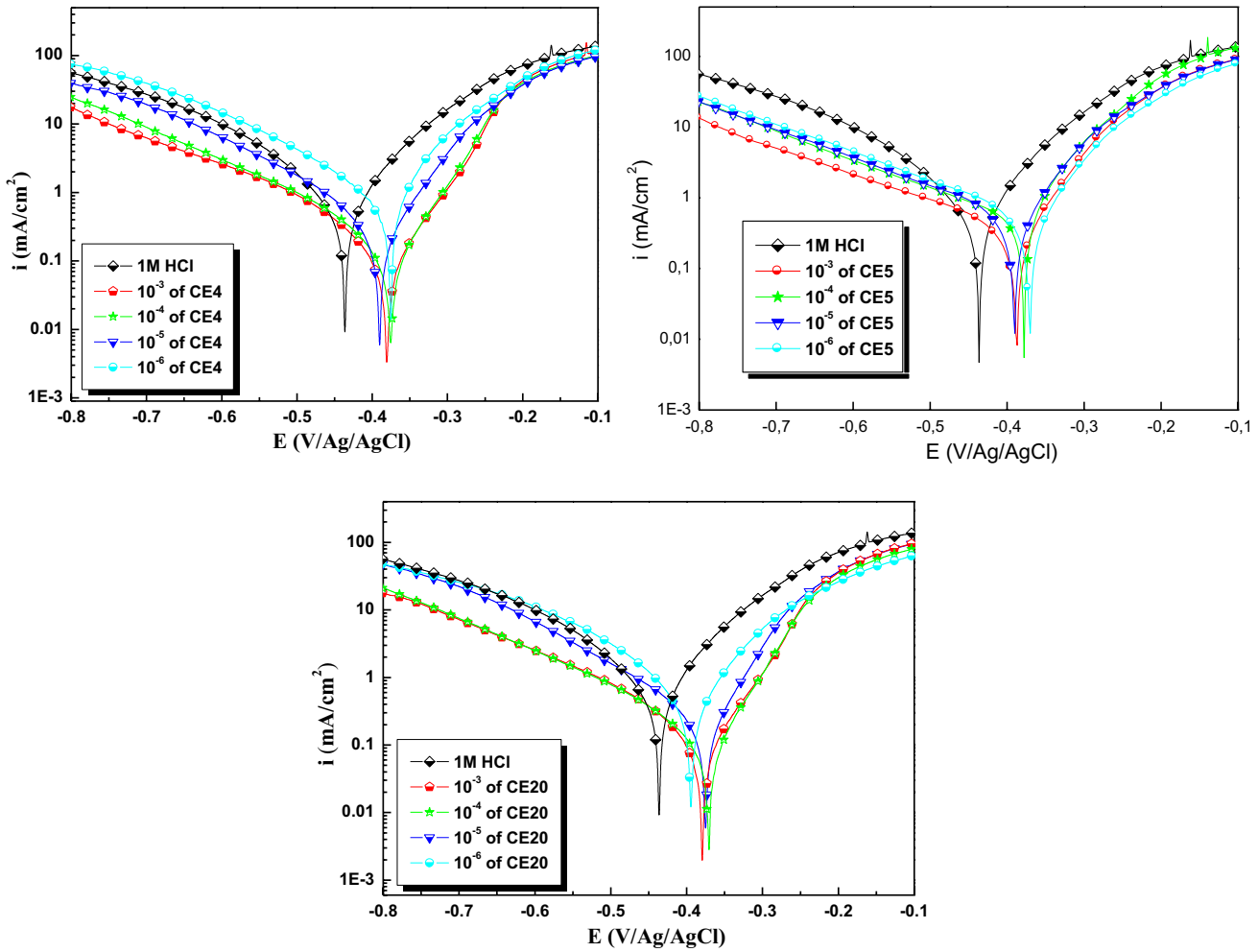

Fig. 1 Polarization curves for MS exposed to various corrosive solutions at 298 K

From Table 3 we notice that the addition of CE4, CE5, and CE20 had a negligible effect on the cathodic Tafel slopes (βc), indicating that the adsorption does not imply a change in the mechanism of cathodic reaction [17, 18].

It is evident that the studied inhibitors compounds act as corrosion inhibitors by getting adsorbed onto MS by simply blocking the active sites, and these results point out that the addition of the inhibitors reduces the anodic dissolution and also retards the cathodic hydrogen evolution reaction, indicating that this inhibitors exhibit a mixed-type inhibition effect. Further, it is also observed that the addition of inhibitors caused as a light shift of the corrosion potential (E_{corr}) toward more electropositive values. According to the literature, If the displacement of E_{corr}(inh) in regard to the E_{corr} blank solution is higher than ± 85 mV, the inhibitor can be considered as a cathodic or anodic type [1, 2].

The decreases in the corresponding current densities and the increase in the degree of surface coverage (θ) with increasing inhibitors concentrations through the formation of anodic protective films on the electrode surface [19] affirm that these compounds perform as corrosion inhibitors for MS dissolution. The inhibition efficiency can be arranged at the optimum concentration of 10^{-3} M in the order: CE20 (88%) > CE4 (86%) > CE5 (77%). The order of inhibitory efficacy increases with the number of nitrogen (N) heteroatoms. The presence of several heteroatoms in the molecule promotes electron sharing which reflects its higher reactivity. In addition, this order of effectiveness changes at the concentration of 10^{-6} M:CE5 > CE20 > CE4. Therefore, there is the probability that CE20 and CE4 compounds can be degraded with strong dilution. These results indicate that the pyridine ring is more resistant to degradation compared to the pyrimidine and tetrazole ring.

3.3 EIS Measurements

This method is considered an efficient analytical tool for the evaluation of the nature of corrosion inhibitors on the metal without disturbing the double layer at the MS/solution interface. Inhibitory behavior of MS in 1 M HCl solution with various concentrations of **CE4**, **CE5,** and **CE20** inhibitor was identified by EIS at 298 K after 30 min of immersion. The Nyquist diagrams are depicted in Fig. 2.

The Nyquist plots display a single semicircle capacitive loop at all the studied concentrations of inhibitors. By increasing the concentration of inhibitors, the diameter of the capacitive loops increases, indicating that the MS corrosion is related to the charge transfer process. Furthermore, the capacitive semicircle loop is depressed under the real axis, which is mainly related to the frequency dispersion effect of irregular and rough electrode surface [20, 21]. Hence, the perfect double layer is not formed and double-layer capacitance (C_{dl}) can be replaced by constant phase element (CPE) with surface regularity factor (n_{dl}).

The experimentally obtained plots were fitted using the simple Randel circuit Fig. 3, which includes three elements, Rs (solution resistance), CPE and R_{ct} (charge transfer resistance). The proposed model exactly fits the experimental results.

The electrochemical parameters of impedance involving charge transfer resistance (R_{ct}), double-layer capacitance (C_{dl}) and inhibition efficiency (IE_{imp}, %) determined from this technique are registered in Table 4.

According to Table 4, it should be pointed that C_{dl} decreases and R_{ct} increases with the inhibitor concentrations increasing. The decrease in the value of the double-layer capacitance may be in accordance with the increase in the thickness of the electrical double layer or the decrease in the local dielectric constant, illustrating the adoption process of these compounds on the surface of the MS. The increase in charge transfer resistance results from the formation of a barrier film on the MS interface [22]. These results are approved by those obtained by the Potentiodynamic polarization. The inhibition efficiencies recorded by EIS at the maximum concentration are **85%** for CE4 and CE20 and **75%** for CE5. The high inhibitive properties of these compounds are mainly due to the availability of their π-electrons of –C=N azomethine double bond, –OH and methyl functional groups, which can coordinate with metals to form a barrier between the metal and corrosive elements [23] (Table 5).

3.4 Adsorption Isotherm and Thermodynamic Parameters

The adsorption isotherms afford important information about the exchanges inhibitor molecules/metal surface. To show maximum adherence of an inhibitor to an appropriate model and the assumptions upon which it was derived, the slope of the plot should be unity. It is believed that the closer the slope is to unity, the more likely the inhibitor obeys the isotherm model.

The adsorption isotherm models are given by the following equation:

$$\text{KC}_{\text{inh}} = \frac{\theta}{1-\theta}; \quad \frac{C_{\text{inh}}}{\theta} \text{ versus } C_{\text{inh}} \quad \text{(Langmuir isotherm)} \tag{4}$$

$$e^{(-2f\theta)} = \text{KC}_{\text{inh}}; \quad \theta \text{ versus } \ln(C_{\text{inh}}) \quad \text{(Temkin isotherm)} \tag{5}$$

$$\theta = \text{KC}_{\text{inh}}^{n}; \quad \ln(\theta) \text{ versus } \ln\left(C_{\text{inh}}\right) \quad \text{(Freundlich isotherm)} \tag{6}$$

$$\frac{\theta}{1-\theta} e^{(-2f\theta)} = \text{KC}_{\text{inh}}; \quad \theta \text{ versus } \ln\left(C_{\text{inh}} \frac{1-\theta}{\theta}\right) \quad \text{(Frumkin isotherm)} \tag{7}$$

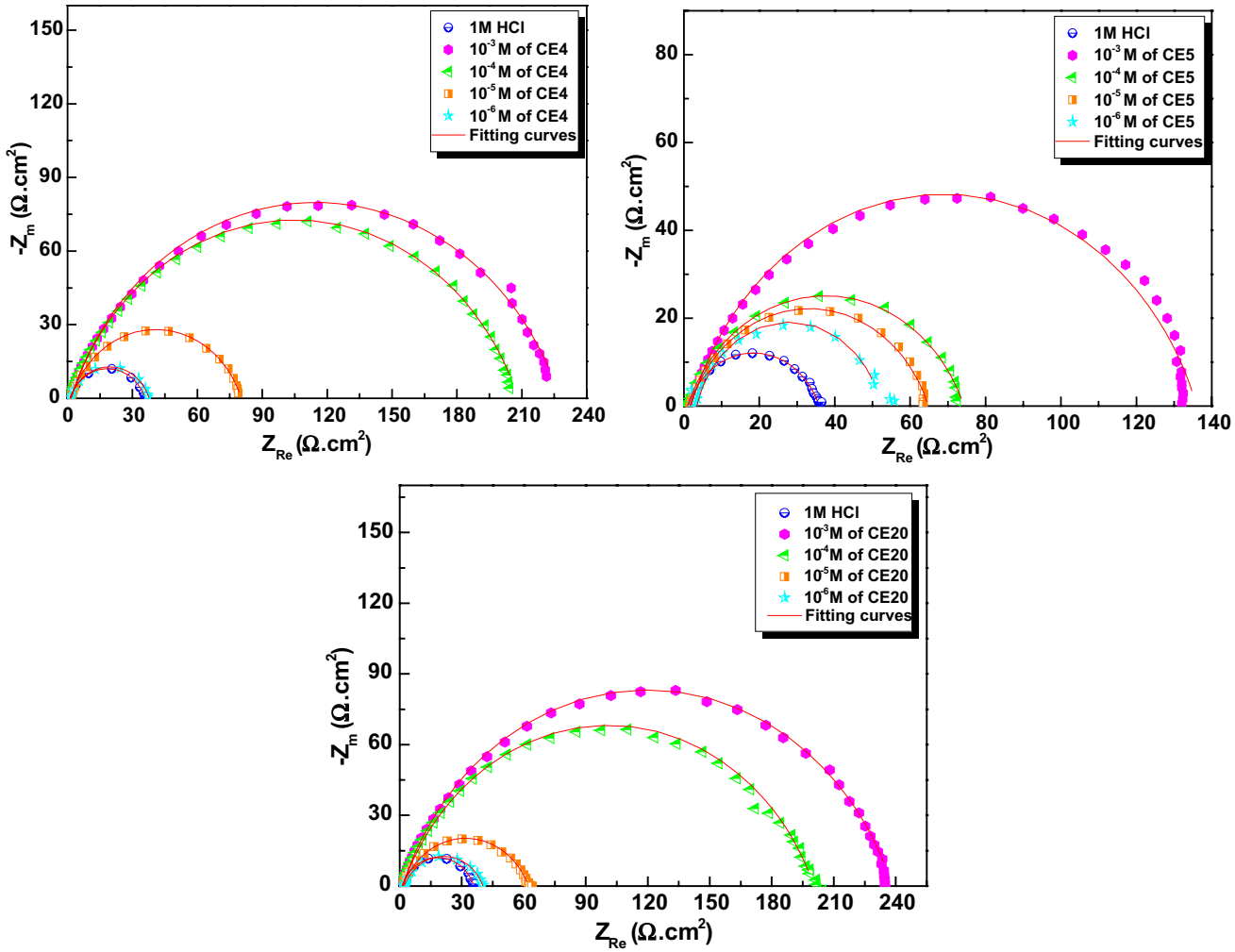

Fig. 2 EIS diagrams of MS immersed in diverse concentrations of inhibitors at 298 K

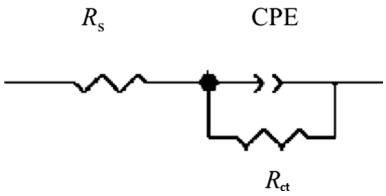

Fig. 3 Randel Electrical equivalent circuit

The experimental data obtained from electrochemical frequency modulation measurements were applied to different adsorption isotherm equations such as Langmuir, Freundlich, Temkin, and Frumkin (Fig. 4). The fitted linear regression coefficients (R^2) as well as the slopes close to unity indicate that the adsorption of all studied compounds on the mild steel surface is accord to the Langmuir isotherm, which is explained by a single-layer characteristic [24, 25]. The adsorption isotherm relationship of Langmuir is represented by Eq. (8) [26, 27]:

$$\frac{C_{\text{inh}}}{\theta} = C_{\text{inh}} + \frac{1}{K} \tag{8}$$

where C_{inh} is the inhibitor concentration, K is the equilibrium constant of the adsorption/desorption process and θ is the surface coverage of inhibitor.

It seems evident from Fig. 4 that the plot of the linear fit is a straight line with a standard coefficient of regression and a slope value proximately unity which confirms that the Langmuir isotherm model is the most adequate for the three inhibitors.

The value of the equilibrium constant, K_{ads}, which can be determined from the reciprocal of the intercept of C/θ-axis is used to estimate the standard free energy of inhibitor adsorption, ΔG^0_{ads}, on the metal surface. The following equation is reported for the calculation of ΔG^0_{ads} at different temperatures.

The free energy of adsorption (ΔGads) is calculated using Eq. (9) [28, 29]:

Table 4 Impedance parameters for MS in diverse concentrations of inhibitor compounds at 298 K

Medium	Concentration (M)	R_s (Ω cm^2)	R_{ct} (Ω cm^2)	C_{dl} (μF cm^{-2})	n_{dl}	Q (μF S^{n-1})	Θ	IE$_{imp}$ (%)
1 M HCl	–	1.09	***35***	121	0.769	427	–	–
CE4	10^{-3}	1.56	***226***	33	0.782	97	0.845	***85***
	10^{-4}	1.52	***207***	43	0.780	121	0.831	***83***
	10^{-5}	1.52	***79***	62	0.788	191	0.556	***56***
	10^{-6}	1.17	***37***	85	0.776	309	0.054	***05***
CE5	10^{-3}	1.57	***138***	54	0.773	165	0.746	***75***
	10^{-4}	0.82	***74***	60	0.757	223	0.527	***53***
	10^{-5}	1.48	***64***	74	0.768	255	0.453	***46***
	10^{-6}	2.55	***50***	64	0.824	175	0.300	***30***
CE20	10^{-3}	1.46	***236***	34	0.782	97	0.852	***85***
	10^{-4}	1.51	***198***	42	0.767	127	0.823	***82***
	10^{-5}	1.42	***61***	73	0.748	285	0.426	***43***
	10^{-6}	2.14	***38***	85	0.744	368	0.078	***08***

The values of the parameters marked in bolditalics are related to each other and have a significance on the protective power of the two products

Table 5 Equilibrium constant and ΔG^0_{ads} values for MS 1 M HCl in the existence and nonexistence of studied compounds at 298 K

Inhibitor	K (L mol^{-1})	ΔG^0_{ads} (kJ mol^{-1})
CE4	1.50×10^5	−42.22
CE5	5.39×10^5	−40.69
CE20	1.5×10^4	−40.07

$$\Delta G_{ads} = -RT\ln(55.5\ \mathrm{K}) \tag{9}$$

where R is the gas constant ($R = 8.314$ J mol^{-1} K^{-1}), T is the absolute temperature (K) and the factor 55.5 is the $C_{(H2O)}$ in mol/L.

It is believed that an inhibitor molecule is physically adsorbed by generating an electrostatic interaction between the charged molecules and the metal if the free energy values are around − 20 kJ mol^{-1} [29], whereas values close to − 40 kJ mol^{-1} or higher indicate the formation of a coordinated covalent bond explained by a chemical adsorption process that involves the transfer (or sharing) of electrons between the inhibitor molecules and the surface of the metal [30]. Values of ΔG^0_{ads} calculated for CE4, CE5 and CE20 are − 42.22, − 40.69 and − 40.07 kJ mol^{-1}, respectively. It is thus evident that the Schiff Base compounds chemically adsorb on MS surface at ambient temperature in acidic media with the help of a coordinate bond formed between the investigated inhibitor molecules and the surrounding *d*-orbital of the surface of mild steel through lone pair of electrons of N, and O atoms.

3.5 Temperature Effect and Thermodynamic Parameters

The temperature outcome on the corrosion inhibition of MS in acidic solutions in the absence and presence of various concentrations of the Schiff's base inhibitors studied was tested using polarization experiments over a temperature range from (298 to 322 K) and shown in Fig. 5. The corresponding parameters (E_{corr}, i_{corr}, bc, and IE$_{PP}$) collected from the curves are listed in Table 6. These results reveal that the increase in temperature has a slight influence on the corrosion inhibition of MS in the presence of inhibitors compared to the blank solution. It can be deduced that the dissolution of the metal takes place by a chemical adsorption process involving strong interactions between the different inhibitors and the surface of MS.

Table 6 shows that the increase in the temperature decreases the inhibition efficiency of the three inhibitors as a consequence of a partial desorption of the inhibitor's molecules from the metal surface.

The energy of activation (Ea) was estimated using the Arrhenius Eq. (10) and registered in Table 7 [31]:

$$\mathrm{Ln}\, i_{corr} = -\frac{E_a}{RT} \tag{10}$$

where T is the absolute temperature, and R is the gas constant.

The enthalpy and entropy of activation (ΔH^* and ΔS^*) could be determined through the alternative formulation of the Arrhenius Eq. (11) [32, 33]:

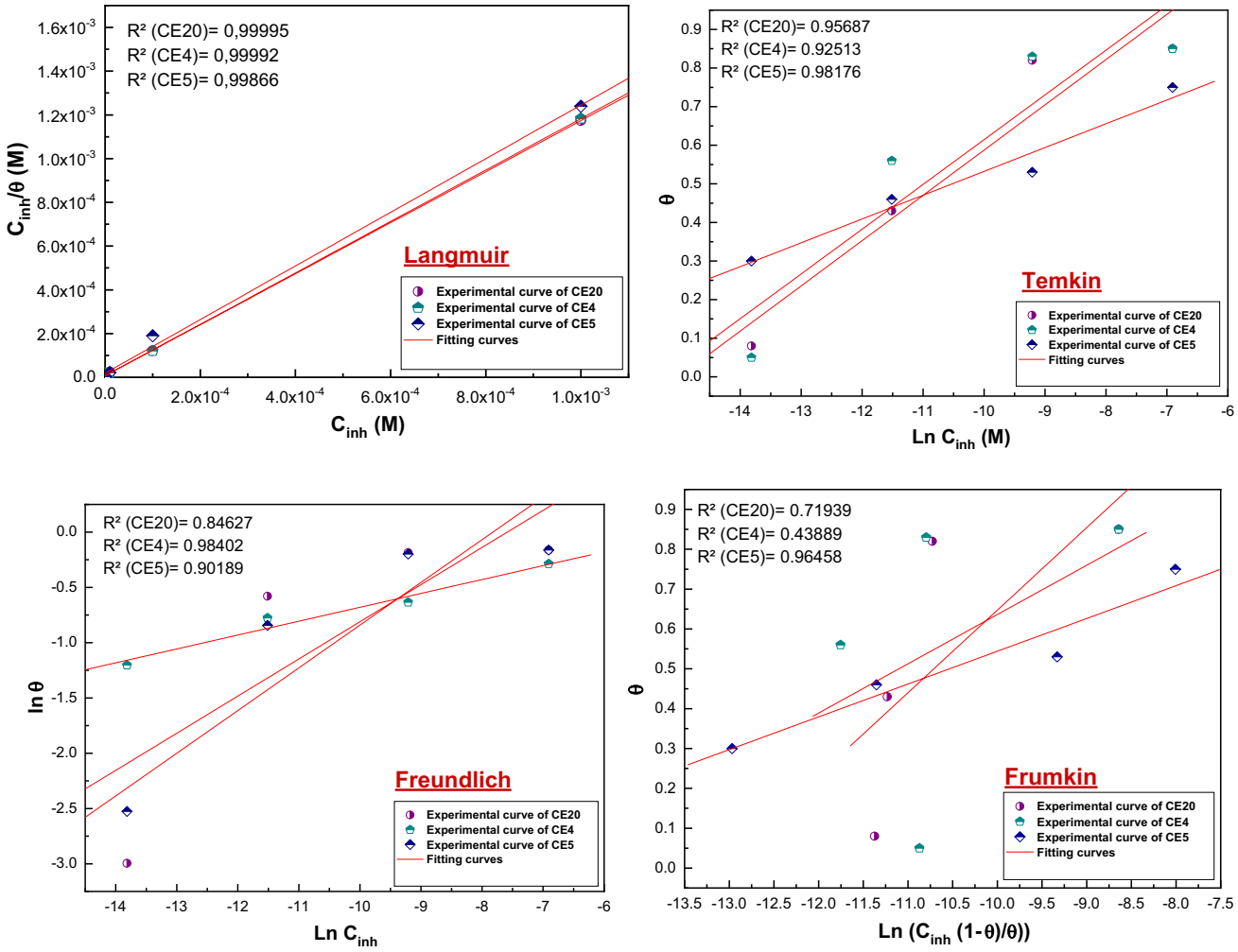

Fig. 4 Langmuir, Temkin, Freundlich, and Frumkin models for the adsorption of CE20, CE4 and CE5 on MS surface in 1 M HCl at 298 K

$$\mathrm{Ln}\frac{i_{\mathrm{corr}}}{T} = \frac{RT}{Nh} e^{\frac{\Delta S*}{R}} e^{-\frac{\Delta H*}{RT}} \tag{11}$$

where N refers to Avogadro's number, and h is the Plank's constant.

Figure 6 presents the variation in the logarithm of the corrosion rate as a function of 1000/T for different concentrations. Figure 7 illustrates the change in Ln i_{corr}/T versus 1000/T. As can be seen, straight lines fit are given for all studied inhibitors. The obtained results are compiled in Table 7.

From the results of Table 7 we observe an increase in the Ea in the presence of the optimum concentration for the various inhibitors studied when compared to that in its absence, this increase can be interpreted as a process of adsorption of physical nature which by forming electrostatic bonds. The $\Delta H*$ values are positive for the three studied inhibitors; this implies that the adsorption of the inhibitors molecules on MS is controlled by an endothermic process. [34].

Moreover, an inspection of $\Delta S*$ data shows that the activation entropies obtained in the presence of inhibitors are greater than those in the absence of inhibitors. The negative values of $\Delta S*$ imply a decrease in the disorder when the reagents are transformed into an activated complex [35]. Inhibitor molecules might freely move in the blank solution before they adsorb onto the MS but with the progress in the adsorption, inhibitor molecules were orderly adsorbed on the mild steel surface which involves an entropy decrease. It is believed that since the adsorption is an exothermic process there must be a decrease in entropy [37, 39].

3.6 Surface Analysis

For the surface characterization, scanning electron microscopy (SEM) is a powerful tool to examine the morphology of the metal surface and the accumulation of the corrosion products on the corroded specimens. Figure 8a–e SEM image of (a): mild steel, (b): Blank immersed at 1 M HCl,

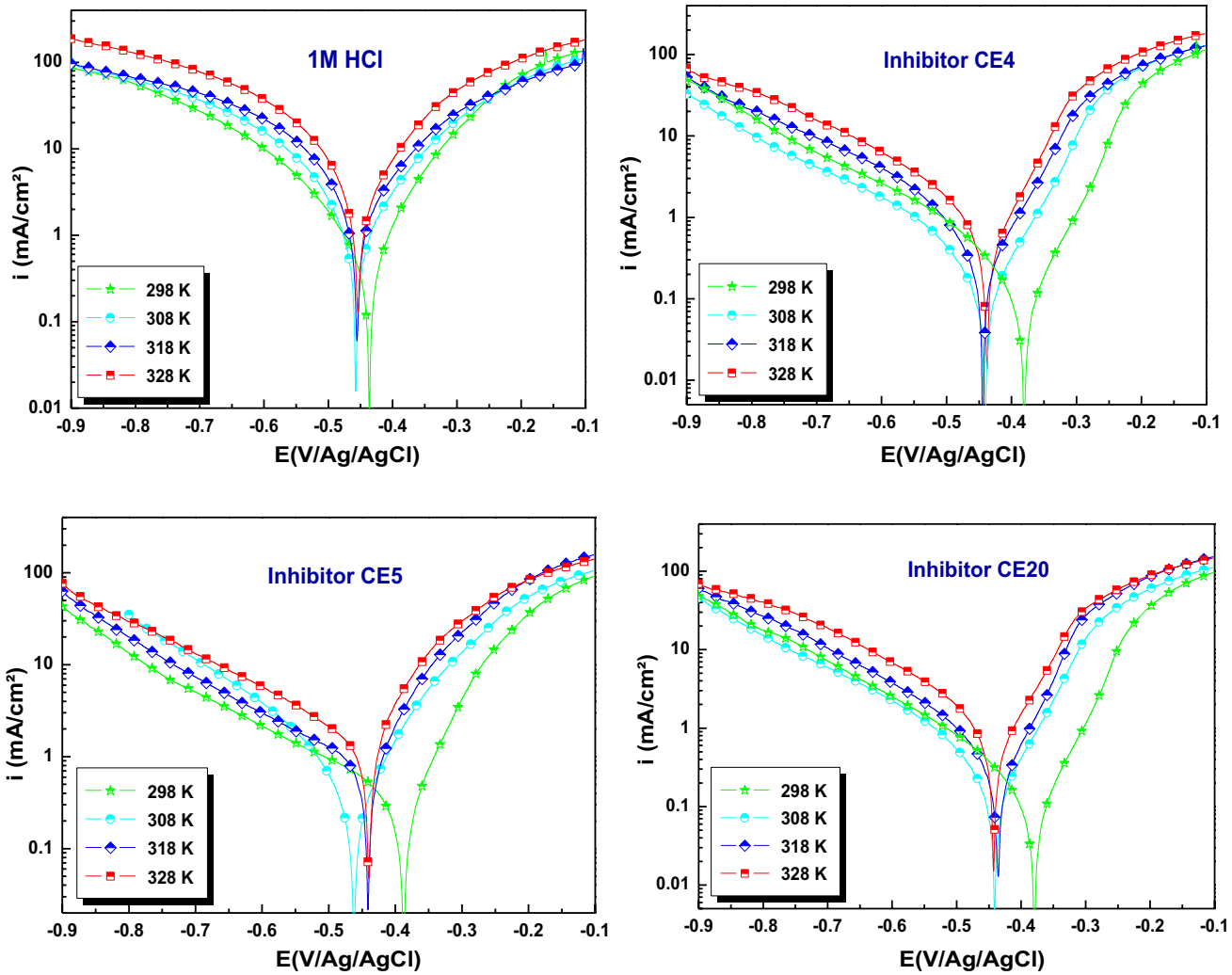

Fig. 5 Polarization curves of the Blank solution and the solutions with the presence of the effective concentrations of CE4, CE5, and CE20

(c): 10^{-3} M of CE4 inhibitor, (*d*): 10^{-3} M of CE5 inhibitor and (e): 10^{-3} M of CE20 inhibitor, respectively, shows the SEM image of uninhibited and inhibited mild steel specimens in 1 M HCl for 6 h of the immersion at the effective concentration of the Schiff base inhibitors.

We observe that the surface is relatively smooth for the MS inhibited specimens, whereas the surface of the uninhibited mild steel specimen is highly corroded by reason of acid attack [30, 31]. This proves that the inhibition is done through the formation of an adsorbed film of the Schiff base molecules on the metal surface.

3.7 Evaluative Study Via Quantum Chemical Calculations

This study was undertaken to establish the relationship between the electronic properties of molecular structure and the corresponding inhibitive effect on the MS surface. Figure 8 shows optimized geometry structures of HOMO: Highest Occupied Molecular Orbital and LUMO: Lowest Unoccupied Molecular orbital of the studied compound. The geometrically optimized structure and electronic properties (E_{HOMO}, E_{LUMO}, total energy, dipole movement) are obtained by DFT method and other quantum chemical parameters such as energy gap (ΔE), total energy, dipole moment (μ), global hardness (η), softness (σ), electronegativity (χ) and fraction of electrons transferred from the inhibitor molecule to the metal surface (ΔN) are summarized in Table 9. The different parameters are calculated by the following equations [40–43].

$$\Delta E_{gap}\,(\mathrm{eV}) = E_{LUMO} - E_{HOMO} \tag{12}$$

$$\chi = \frac{1}{2}\left(E_{HOMO} + E_{LUMO}\right) \tag{13}$$

Table 6 Polarization parameters and corresponding inhibition efficiencies for CE4, CE5 and CE20 in 1 M HCl solution at various temperatures

Medium	Temperature (K)	$-E_{corr}$ (mV/Ag/AgCl)	i_{corr} (μA cm^{-2})	$-\beta_c$ (mV dec^{-1})	IE$_{PP}$ (%)
1 M HCl	298	436	***694***	139	–
	308	457	***910***	105	–
	318	454	***1300***	93	–
	328	452	***1991***	94	–
CE4	298	381	***98***	114	***86***
	308	440	***147***	129	***84***
	318	444	***222***	105	***82***
	328	437	***370***	104	***81***
CE5	298	387	***163***	112	***77***
	308	462	***246***	93	***73***
	318	438	***389***	98	***70***
	328	439	***700***	109	***65***
CE20	298	380	***84***	118	***88***
	308	441	***174***	129	***81***
	318	436	***294***	114	***77***
	328	442	***558***	132	***72***

The values of the parameters marked in bolditalics are related to each other and have a significance on the protective power of the two products

Table 7 Dissolution parameters of MS in in corrosive solution with and without the addition of the inhibitor's CE4, CE5, and CE20 effective concentrations

Medium	E_a (KJ mol^{-1})	ΔH^* (KJ mol^{-1})	ΔS^* (J mol^{-1} K^{-1})
1 M HCl	30.38	27.69	− 113.32
10^{-3} M of CE4	38.01	35.33	− 104.68
10^{-3} M of CE5	41.72	39.04	− 88.58
10^{-3} M of CE20	53.76	51.08	− 54.40

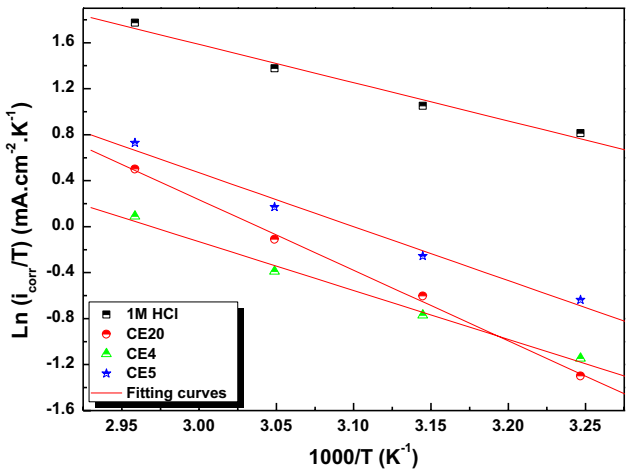

Fig. 6 Arrhenius plots of MS in corrosive solution with and without the addition of the inhibitor's CE4, CE5, and CE20 effective concentrations

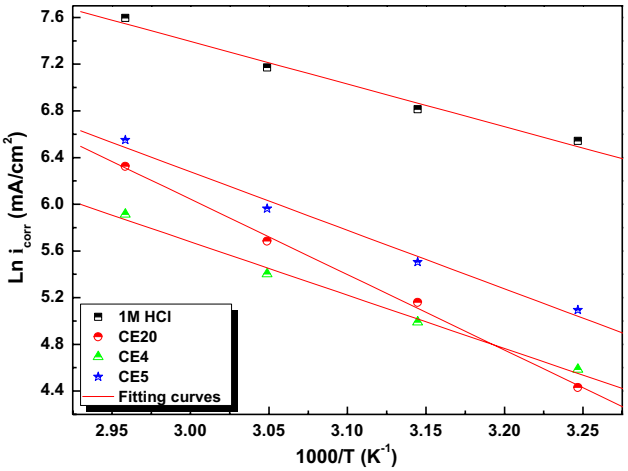

Fig. 7 Transition state plots of MS in corrosive solution with and without the addition of the inhibitor's CE4, CE5, and CE20 effective concentrations

$$\eta = \frac{1}{2}\left(E_{HOMO} - E_{LUMO}\right) \tag{14}$$

$$\sigma = \frac{1}{\eta} \tag{15}$$

$$\Delta N = \frac{\chi_{Fe} - \chi_{inh}}{2\left[\eta_{Fe} + \eta_{inh}\right]} \tag{16}$$

where χ_{Fe} and η_{Fe} are the absolute electronegativity and hardness of the metal, respectively.

χ_{inh} and η_{inh} are the absolute electronegativity, and the absolute hardness of the inhibitor molecule, respectively.

The HOMO value is higher in the zone to the ester oxygen and nitrogen, which is attributed to the possession of the inhibitor's atoms O and N of a lone pair of electrons. Hence, the preferred active sites for donating electrons are mainly located within the regions around oxygen and nitrogen atoms. The LUMO densities are higher on the pyridine region, indicating the preferred active sites for accepting electrons. Thereby it is reasonable to assume that the ester oxygen donates electrons and form strong interaction with unoccupied *d*-orbitals of metal. The interaction of inhibitor and metal surface can occur based on donor–acceptor interactions [44]. Table 8 shows the higher value of E_{HOMO} indicating a tendency to sharing electrons with suitable acceptors that have vacant molecular orbital. The lower value of ELUMO indicates the ability to accept an electron from a donor molecule [45]. The E_{HOMO} value of iron is Fe (− 0.201 eV), Fe^{+2} (− 1.001 eV), and Fe^{+3} (− 1.765 eV) which is less than that of the inhibitor molecules (− 6.29, − 6.73, − 6.92 eV).

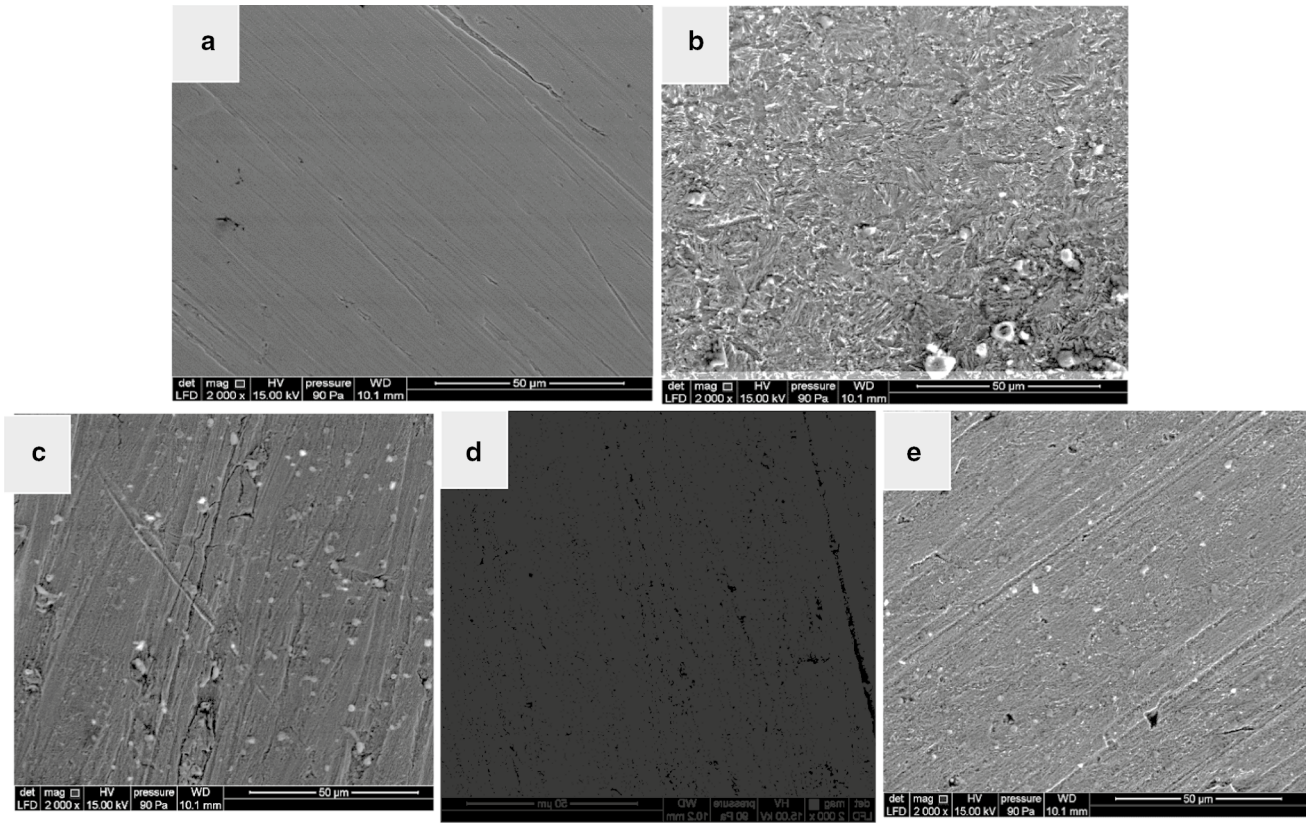

Fig. 8 SEM of MS: **a** polished; **b** immersed in 1 M HCl for 6 h; **c** immersed in 10^{-3} M of CE4, **d** immersed in 10^{-3} M of CE5 and **e** immersed in 10^{-3} M of CE20

Table 8 Quantum chemical parameters for neutral molecules of CE4, CE5, and CE20 calculated with DFT/B3LYP/6-31G (*d*,*p*) method in a gas phase

Parameters	CE5	CE4	CE20
E_{HOMO} (eV)	−6.2982	−6.7363	−6.9232
E_{LUMO} (eV)	−0.8650	−1.1720	−1.5562
ΔE_{gap} (eV)	5.4331	5.5643	5.3670
η (eV)	2.7165	2.7821	2.6835
σ (eV^{-1})	0.3681	0.3594	0.3726
χ (eV)	3.58164	3.9541	4.2397
ω	2.3610	2.8099	3.3492
ε	0.4235	0.3558	0.2985
ΔN	0.6291	0.5473	0.5142
μ (D)	3.7040	2.7129	5.2068

Hence it is clear that the inhibitor molecules donate electrons to the metal. The energy gap between E_{HOMO} and E_{LUMO} is referred to as ΔE. Lower energy gap means easy jumping of electron HOMO to LUMO of the other molecule, which may result in high efficiency values [46]. In addition, it can be seen in Table 8 that EC20 has the highest value of softness (0.3726) and the lowest value of hardness (2.6835), which indicates that this compound is the most reactive compared to the other compounds [47]. Electronegativity (χ) is the measure of the power of an electron or group of atoms to attract electrons toward itself [48]. The calculated electronegativity values presented in (Table 1) show that CE20 has higher χ value than CE4 and CE5. This implies that CE20 has a higher power to attract electrons to itself and hence a better corrosion inhibitor. The electrophilicity (ω) and nucleophilicity (ε) are chemical reactivity descriptors that provide the capacity of the molecule to receive and release electrons. In our case, the inhibitor CE20 with high electrophilicity value and low nucleophilicity value than the other compounds, has the highest inhibition efficiency.

The high dipole moment values are linked to high inhibition efficiency resulting from the large dipole inhibitor's molecule and the metal surface interaction, all inhibitors have higher dipole moments compared to water (1.8 D), and hence they easily displace water molecule from the metal surface [49]. According to the literature [40, 44, 46] if ΔN

is less than 3.6 the inhibitor has the tendency to donate an electron to the mild steel surface. In this, study the values of ΔN are less than 3.6 for all the inhibitors which confirm that the three inhibitors strongly interact with the metal surface [50, 51]. All these calculations correlated the experimental results.

The local reactivity of the studied inhibitors is investigated using the condensed Fukui indices which are an indication of the reactive centers of molecules (nucleophilic and electrophilic centers) [49]. Electrophilic f_k^- and nucleophilic f_k^+ attacks are calculated using Eqs. (17) and (18) [52]:

$$\text{For nucleophilic attack}: \quad f_k^+ = P_k(N+1) - P_{_k}(N) \tag{17}$$

$$\text{For electrophilic attack}: \quad f_k^- = P_k(N) - P_k(N-1) \tag{18}$$

Table 9 includes the values of the Fukui functions for the three molecules after a nucleophilic and electrophilic attack. Analysis of this results shows that the highest values of f_k^+ are localized on the atoms C7 and N6 for the molecule CE20, on the atoms C2, C6 and N1 for the molecule CE4 and on the atoms C2, C3, C6, C8 and N1 for the molecule CE5 which argues that these sites are electrons acceptors, while the high values of f_k^- are shown on the atoms O12 and N6 for the molecule CE20 and the atoms O13 and N7 for both the atoms CE5 and CE4 which implies that these sites are electrons donor. These results explain the high adsorption of those molecules on the MS surface [53].

3.8 Monte Carlo (MC) Simulation

In order to better understand the adsorption behavior of the inhibitors tested. We have considered Monte Carlo simulations of the inhibitor molecules on Fe (110) surface in the presence of water molecules. The most stable low-energy adsorption patterns of CE5, CE4 and CE20 inhibitors on Fe (110)/100 H2O molecule system are shown in Fig. 9.

In general, the mechanism of corrosion inhibition is by adsorption [54]. It is clear from the absolute value of the adsorption energies of studied inhibitors on the iron surface in the presence of water follows the order: CE20 > CE5 > CE4. This ordering also corroborates with the result obtained by experimental Techniques and DFT method. In all studied systems, the adsorption energies of the inhibitors are far higher than that of H_2O molecules (Table 10) and reflect the possibility of gradual substitution of H_2O molecules from the Fe (110) surface [55], indicating a great capacity of these molecules to form a protective film by adsorption on the surface of Mild steel [56, 57] (Fig. 10).

4 Conclusions

The undertaken experimental and theoretical studies on the corrosion inhibitive action of novel Schiff base compounds on mild steel in 1 M HCl solution were investigated. The results obtained lead to the conclusion that CE4, CE5, and CE20 act effectively in reducing the corrosion rate of mild steel in corrosive solutions. Increasing the concentrations of these inhibiting compounds increases their inhibiting effectiveness to its highest value (88%) at 10^{-3} M of CE20. The potentiodynamic polarization curves indicate that the studied Schiff's base

Table 9 Fukui functions of the Schiff's base inhibitors CE4, CE5, and CE20

Inhibitor	Atom k	$P\,(N)$	$P\,(N+1)$	$P\,(N-1)$	f_k^+	f_k^-
CE 5	1 N	7.48268	7.59011	7.4696	0.10743	0.01308
	2 C	5.92461	6.03574	5.90503	0.11113	0.01958
	3 C	5.56215	5.69649	5.57564	0.13434	−0.01349
	6 C	6.12641	6.3081	6.11087	0.18169	0.01554
	7 N	7.48919	7.49707	7.30376	0.00788	0.18543
	8 C	5.61647	5.73312	5.5806	0.11665	0.03587
	13 O	8.5401	8.54284	8.2865	0.00274	0.2536
CE 4	1 N	7.50123	7.61299	7.48626	0.11176	0.01497
	2 C	5.88517	6.05421	5.8696	0.16904	0.01557
	6 C	5.86742	6.08908	5.85336	0.22166	0.01406
	7 N	7.51176	7.51454	7.34795	0.00278	0.16381
	13 O	8.53936	8.54067	8.26818	0.00131	0.27118
CE 20	6 N	7.5002	7.62218	7.30211	0.12198	0.19809
	7 C	5.63764	5.88652	5.59282	0.24888	0.04482
	12 O	8.54103	8.54613	8.30448	0.0051	0.23655

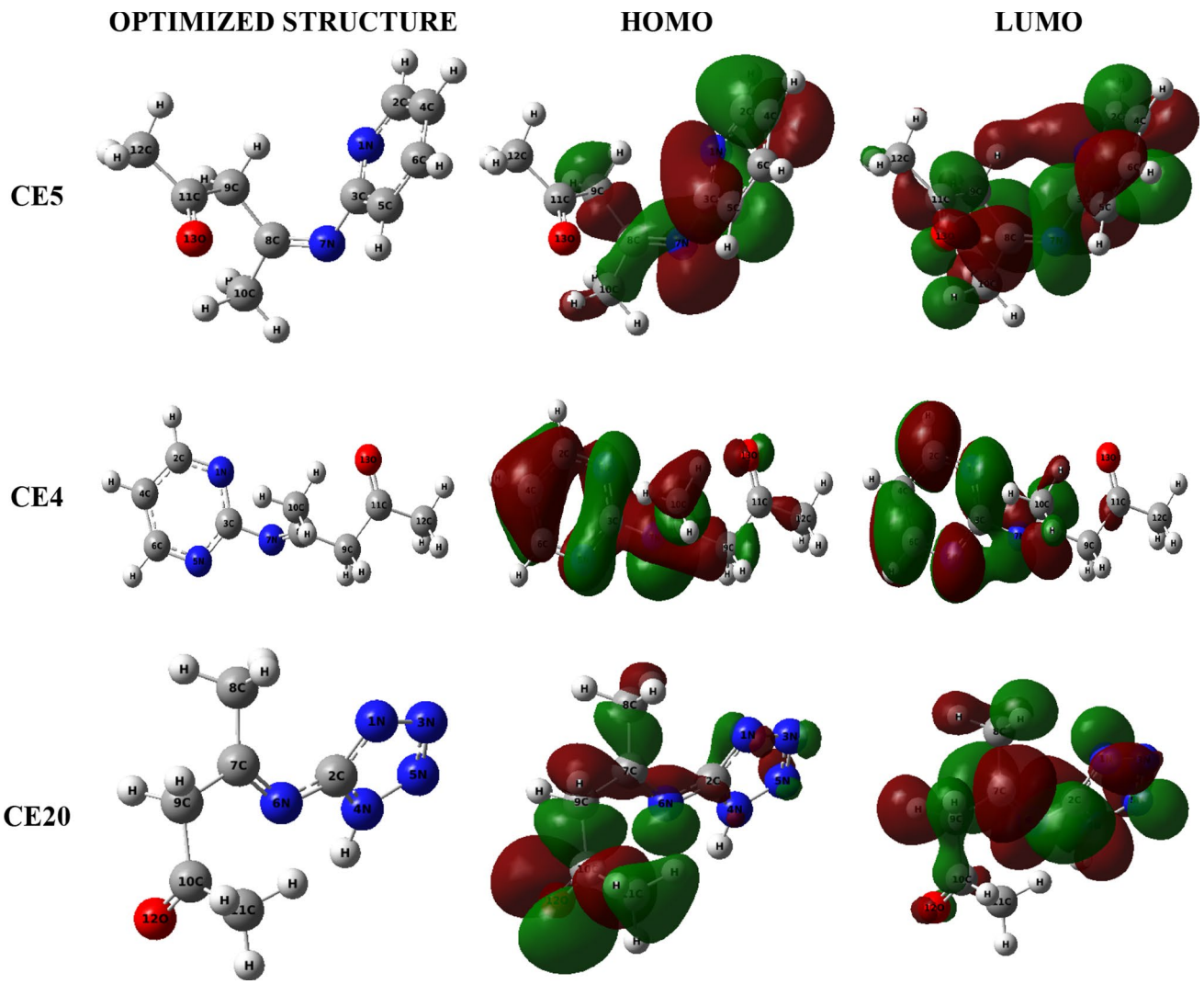

Fig. 9 Optimized structure, HOMO and LUMO energies of CE4, CE5, and CE20

Table 10 Adsorption energies for studied inhibitors on Fe(110)/100H_2O system obtained using the Monte Carlo simulation (all units in kcal/mol)

Systems	Adsorption energy inhibitor	Adsorption energy water
Fe(110)/CE4/100H_2O	− 1656.83	− 14.12
Fe(110)/CE5/100H_2O	− 1657.02	− 12.62
Fe(110)/CE20/100H_2O	− 1675.69	− 15.48

molecules are of a mixed type. The impedance graphs show that the studied inhibitors have a higher inhibition performance is related to high values of charge transfer resistance which arises from the adsorption on the metal surface. The adsorption of inhibitor molecules on the surface of mild steel results in the formation of a barrier film that blocks the reaction sites following Langmuir adsorption isotherm in our case. Surface analysis confirms the presence of a protective layer formed on the surface of

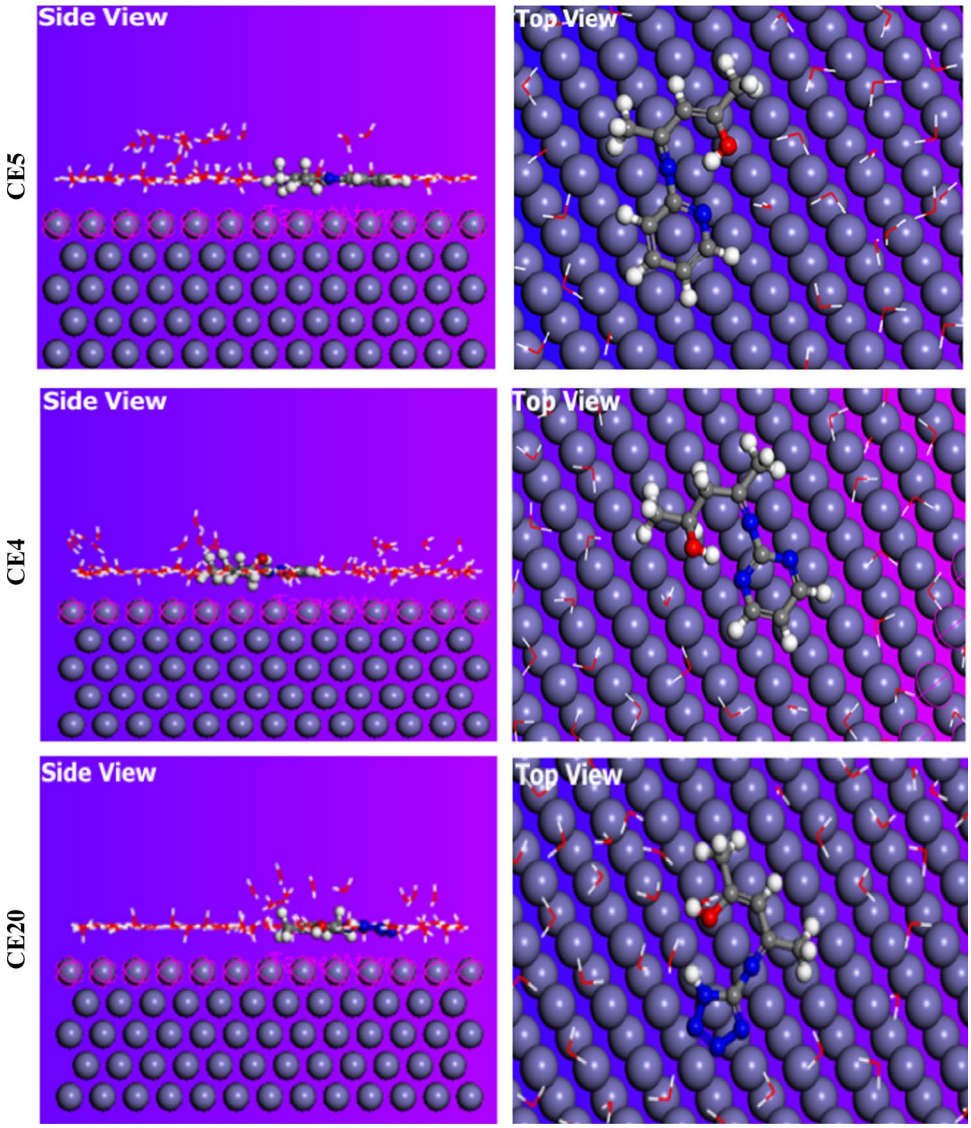

Fig. 10 Most stable low energy configuration for the adsorption of studied inhibitors on Fe (110)/100H_2O system obtained using the Monte Carlo simulation

MS. The theoretical studies are in agreement with the experimental ones.

Compliance with Ethical Standards

Conflict of interest The authors declare that they have no conflict of interest.

References

1. Olasunkanmi, L.O.; Kabanda, M.M.; Ebenso, E.E.: Quinoxaline derivatives as corrosion inhibitors for mild steel in hydrochloric acid medium: electrochemical and quantum chemical studies. Phys. E Low-dimens. Syst. Nanostruct. **76**, 109–126 (2016)
2. El Kacimi, Y.; Azaroual, M.A.; Touir, R.; Galai, M.; Alaoui, K.; Sfaira, M.; Ebn Touhami, M.; Kaya, S.: Corrosion inhibition studies for mild steel in 5.0 M HCl by substituted phenyltetrazole. Euro-Mediterr. J. Environ. Integr. **2**, 1 (2017). https://doi.org/10.1007/s41207-016-0011-8
3. Fergachi, O.; Benhiba, F.; Rbaa, M.; Ouakki, M.; Galai, M.; Touir, R.; Lakhrissi, B.; Oudda, H.; Touhami, M.E.: Corrosion inhibition of ordinary steel in 5.0 M HCl medium by benzimidazole derivatives: electrochemical, UV–visible spectrometry, and DFT calculations. J. Bio-and Tribo- Corros. **5**(1), 21 (2019)
4. El-Hajjaji, F.; Messali, M.; Aljuhani, A.; Aouad, M.R.; Hammouti, B.; Belghiti, M.E.; Chauhan, D.S.; Quraishi, M.A.: Pyridazinium-based ionic liquids as novel and green corrosion inhibitors of carbon steel in acid medium: electrochemical and molecular dynamics simulation studies. J. Mol. Liq. **249**, 997–1008 (2018)
5. Verma, C.B.; Quraishi, M.A.; Singh, A.: 2-Aminobenzene-1,3-dicarbonitriles as green corrosion inhibitor for mild steel in 1 M HCl: electrochemical, thermodynamic, surface and quantum chemical investigation. J. Taiwan Inst. Chem. Eng. **49**, 229–239 (2015)

6. Ahamad, I.; Prasad, R.; Quraishi, M.A.: Inhibition of mild steel corrosion in acid solution by Pheniramine drug : experimental and theoretical study. Corros. Sci. **52**(9), 3033–3041 (2010)
7. Ebenso, E.E.; Kabanda, M.M.; Murulana, L.C.; Singh, A.K.; Shukla, S.K.: Electrochemical and quantum chemical investigation of some azine and thiazine dyes as potential corrosion inhibitors for mild steel in hydrochloric acid solution. Ind. Eng. Chem. Res. **51**(39), 12940–12958 (2012)
8. Guadalupe, H.J.; García-Ochoa, E.; Maldonado-Rivas, P.; Borbolla, J.; Thangarasu, P.: A combined electrochemical and theoretical study of *N*, *N*′-bis(benzimidazole-2yl-ethyl)-1,2-diaminoethane as a new corrosion inhibitor for carbon steel surface. J. Electroanal. Chem. **655**, 164–172 (2011)
9. Bedair, M.A.; El-sabbah, M.M.B.; Fouda, A.S.; Elaryian, H.M.: Synthesis, electrochemical and quantum chemical studies of some prepared surfactants based on azodye and Schi ff base as corrosion inhibitors for steel in acid medium. Corros. Sci. **128**, 54–72 (2017)
10. Abdel-Gaber, A.M.; Masoud, M.S.; Khalil, E.A.; Shehata, E.E.: Electrochemical study on the effect of Schiff base and its cobalt complex on the acid corrosion of steel. Corros. Sci. **51**, 3021–3024 (2009)
11. Kumar, R.; Yadav, O.S.; Singh, G.: Electrochemical and surface characterization of a new eco-friendly corrosion inhibitor for mild steel in acidic media: a cumulative study. J. Mol. Liq. **237**, 413–427 (2017)
12. Oruma, U.S.; Asegbeloyin, J.N.; Eze, F.U.; Chaha, K.F.: Synthesis, characterization and preliminary antimicrobial screening of (2z, 4z)-4-(pyrimidin-2ylimino) pent-2-en-2-ol (pip) and its copper (ii) and chromium (iii) complexes. Int. J. Chem. Sci. **12**, 136–144 (2014)
13. Rbaa, M.; Ouakki, M.; Galai, M.; Berisha, A.; Lakhrissi, B.; Jama, C.; Warad, I.; Zarrouk, A.: Simple preparation and characterization of novel 8-Hydroxyquinoline derivatives as effective acid corrosion inhibitor for mild steel: experimental and theoretical studies. Colloids Surf. A **602**, 125094 (2020)
14. Ben Hmamou, D.; Salghi, R.; Zarrouk, A.; Zarrok, H.; Hammouti, B.; Al-Deyab, S.S.; El Assyry, A.; Benchat, N.; Bouachrine, M.: Electrochemical and gravimetric evaluation of 7-methyl-2-phenylimidazo[1,2-α]pyridine of carbon steel corrosion in phosphoric acid solution. Int. J. Electrochem. Sci. **8**, 11526–11545 (2013)
15. Mourya, P.; Banerjee, S.; Singh, M.M.: Corrosion inhibition of mild steel in acidic solution by *Tagetes erecta* (Marigold flower) extract as a green inhibitor. Corros. Sci. **85**, 352–363 (2014)
16. Materials Studio, Revision 8.0, Accelrys Inc., San Diego, USA (2015)
17. Khattabi, M.; Benhiba, F.; Tabti, S.; Djedouani, A.; El Assyry, A.; Touzani, R.; Warad, I.; Oudda, H.; Zarrouk, A.: Performance and computational studies of two soluble pyran derivatives as corrosion inhibitors for mild steel in HCl. J. Mol. Struct. **1196**, 231–244 (2019)
18. Markhali, B.P.; Naderi, R.; Mahdavian, M.; Sayebani, M.; Arman, S.Y.: Electrochemical impedance spectroscopy and electrochemical noise measurements as tools to evaluate corrosion inhibition of azole compounds on stainless steel in acidic media. Corros. Sci. **75**, 269–279 (2013)
19. El Hajjaji, F.; Abrigach, F.; Hamed, O.; Hasan, A.R.; Taleb, M.; Jodeh, S.; Rodríguez-Castellón, E.; del Valle Martínez de Yuso, M.D.; Algarra, M.: Corrosion resistance of mild steel coated with organic material containing pyrazol moiety. Coatings **8**, 330 (2018)
20. El-Hajjaji, F.; Messali, M.; Martínez de Yuso, M.V.; Rodríguez-Castellón, E.; Almutairi, S.; Bandosz, T.J.; Algarra, M.: Effect of 1-(3-phenoxypropyl) pyridazin-1-ium bromide on steel corrosion inhibition in acidic medium. J. Colloid Interface Sci. **541**, 418–424 (2019)
21. Arrousse, N.; Salim, R.; Al Houari, G.; El Hajjaji, F.; Zarrouk, A.; Rais, Z.; Taleb, M.; Chauhan, D.S.; Quraishi, M.A.: Experimental and theoretical insights on the adsorption and inhibition mechanism of (2E)-2-(acetylamino)-3-(4-nitrophenyl) prop-2-enoic acid and 4-nitrobenzaldehyde on mild steel corrosion. J. Chem. Sci. **132**, 112 (2020)
22. Bao-Yu, L.; Zheng, L.; Guo-Cheng, H.; Yang-Hong, L.: Corrosion inhibition and adsorption behavior of 2-((dehydroabietylamine) methyl)-6-methoxyphenol on mild steel surface in seawater. Thin Solid Films **519**, 7836–7844 (2011)
23. Verma, C.; Olasunkanmi, L.O.; Ebenso, E.E.; Quraishid, M.A.: Substituents effect on corrosion inhibition performance of organic compounds in aggressive ionic solutions: a review. J. Mol. Liq. **251**, 100 (2018)
24. Arrousse, N.; Salim, R.; Kaddouri, Y.; Zarrouk, A.; Zahri, D.; El Hajjaji, F.; Touzani, R.; Taleb, M.; Jodeh, S.: The inhibition behavior of two pyrimidine-pyrazole derivatives against corrosion in hydrochloric solution: experimental, surface analysis and in silico approach studies. Arab. J. Chem. **13**, 5949–5965 (2020)
25. Ech-chihbi, E.; Nahlé, A.; Salim, R.; Benhiba, F.; Moussaif, A.; El-Hajjaji, F.; Oudda, H.; Guenbour, A.; Taleb, M.; Warad, I.; Zarrouk, A.: Computational, MD simulation, SEM/EDX and experimental studies for understanding adsorption of benzimidazole derivatives as corrosion inhibitors in 1.0 M HCl solution. J. Alloys Compd. **844**, 155842 (2020)
26. El-Hajjaji, F.; Merimi, I.; Messali, M.; Obaid, R.J.; Salim, R.; Taleb, M.; Hammouti, B.: Experimental and quantum studies of newly synthesized pyridazinium derivatives on mild steel in hydrochloric acid medium. Mater. Today: Proc. **13**, 822–831 (2019)
27. Ituen, E.; Akaranta, O.; James, A.O.: Evaluation of performance of corrosion inhibitors using adsorption isotherm models: an overview evaluation of performance of corrosion inhibitors using adsorption isotherm models: an overview. Chem. Sci. Int. J. **18**(1), 1–34 (2016)
28. Fdil, R.; Tourabi, M.; Derhali, S.; Mouzdahir, A.; Sraidi, K.; Jama, C.; Zarrouk, A.; Bentiss, F.: Evaluation of alkaloids extract of *Retama monosperma* (L.) Boiss. stems as a green corrosion inhibitor for carbon steel in pickling acidic medium by means of gravimetric, AC impedance and surface studies. J. Mater. Environ. Sci. **9**(1), 358–369 (2018)
29. Ech-chihbi, E.; Belghiti, M.E.; Salim, R.; Oudda, H.; Taleb, M.; Benchat, N.; Hammouti, B.; El-Hajjaji, F.: Experimental and computational studies on the inhibition performance of the organic compound "2-phenylimidazo [1,2-a]pyrimidine-3- carbaldehyde" against the corrosion of carbon steel in 1.0 M HCl solution. Surf. Interfaces **9**, 206–217 (2017)
30. Gutiérrez, E.; Rodríguez, J.A.; Cruz-Borbolla, J.; Alvarado-Rodríguez, J.G.; Thangarasu, P.: Development of a predictive model for corrosion inhibition of carbon steel by imidazole and benzimidazole derivatives. Corros. Sci. **108**, 23–35 (2016)
31. Bouoidina, A.; Chaouch, M.; Abdellaoui, A.; Lahkimi, A.; Hammouti, B.; El-Hajjaji, F.; Taleb, M.; Nahle, A.: Essential oil of "Foeniculum vulgare": antioxidant and corrosion inhibitor on mild steel immersed in hydrochloric medium. Anti-Corros. Methods Mater. **5**(64), 563–572 (2016)
32. Ouakki, M.; Galai, M.; Cherkaoui, M.; Rifi, E.H.; Hatim, Z.: Study on the corrosion inhibition of mild steel in two acidic mediums (HCl 1 M AND H2 SO4 0.5 M) containing apatite. J. Chem. Technol. Metall. **55**(2), 436–448 (2020)
33. Echchihbi, E.; Nahlé, A.; Salim, R.; Oudda, H.; El Hajjaji, F.; El Kalai, F.; El Aatiaoui, A.; Taleb, M.: An investigation into quantum chemistry and experimental evaluation of imidazopyridine derivatives as corrosion inhibitors for C-steel in acidic media. J. Bio- and Tribo-Corros. **5**, 24 (2019)

34. Popova, A.; Sokolova, E.; Raicheva, S.; Christov, M.: AC and DC study of the temperature effect on mild steel corrosion in acid media in the presence of benzimidazole derivatives. Corros. Sci. **45**(1), 33–58 (2003)
35. Yadav, M.; Kumar, S.; Ranjan Sinha, R.; Behera, D.: Experimental and quantum chemical studies on corrosion inhibition performance of benzimidazole derivatives for mild steel in HCl. Ind. Eng. Chem. Res. **52**(19), 6318–6328 (2013)
36. Fouda, A.S.; Ismail, M.A.; EL-Ewady, G.Y.; Abousalem, A.S.: Evaluation of 4-amidinophenyl-2,2′-bithiophene and its aza-analogue as novel corrosion inhibitors for CS in acidic media: experimental and theoretical study. J. Mol. Liq. **240**, 372–388 (2017)
37. Zerga, B.; Hammouti, B.; Ebn Touhami, M.; Touir, R.; Taleb, M.; Sfaira, M.; Bennajeh, M.; Forssal, I.: Comparative inhibition study of new synthesised pyridazine derivatives towards mild steel corrosion in hydrochloric acid. Part-II: thermodynamic proprieties. Int. J. Electrochem. Sci. **7**, 471–483 (2012)
38. Danaee, I.; Gholami, M.; RashvandAvei, M.; Maddahy, M.H.: Quantum chemical and experimental investigations on inhibitory behavior of amino–imino tautomeric equilibrium of 2-aminobenzothiazole on steel corrosion in H_2SO_4 solution. J. Ind. Eng. Chem. **26**, 81–94 (2015)
39. Obot, I.B.; Obi-egbedi, N.O.; Umoren, S.: Adsorption characteristics and corrosion inhibitive properties of clotrimazole for aluminium corrosion in hydrochloric acid. Int. J. Electrochem. Sci. **4**, 863–877 (2009)
40. Ouakki, M.; Rbaa, M.; Galai, M.; Lakhrissi, B.; Rifi, E.H.; Cherkaoui, M.: Experimental and quantum chemical investigation of imidazole derivatives as corrosion inhibitors on mild steel in 1.0 M hydrochloric acid. J. Bio- and Tribo-Corros. **4**, 35 (2018)
41. Salim, R.; Elaatiaoui, A.; Benchat, N.; Ech-chihbi, E.; Rais, Z.; Oudda, H.; El Hajjaji, F.; ElAoufir, Y.; Taleb, M.: Corrosion behavior of a smart inhibitor in hydrochloric acid molar: experimental and theoretical studies. JMES **8**(10), 3747–3758 (2017)
42. Ouakki, M.; Galai, M.; Rbaa, M.; Abousalem, A.S.; Lakhrissi, B.; Ebn Touhami, M.; Cherkaoui, M.: Electrochemical, thermodynamic and theoretical studies of some imidazole derivatives compounds as acid corrosion inhibitors for mild steel. J. Mol. Liq. **319**, 114063 (2020)
43. Hsissou, R.; Dagdag, O.; Abbout, S.; Benhiba, F.; Berradi, M.; El Bouchti, M.; Berisha, A.; Hajjaji, N.; Elharfi, A.: Novel derivative epoxy resin TGETET as a corrosion inhibition of E24 carbon steel in 1.0 MHCl solution. Experimental and computational (DFT and MD simulations) methods. Mol. Liq. **284**, 182–192 (2019)
44. Gosav, S.; Paduraru, N.; Maftei, D.; Birsa, M.L.; Praisler, M.: Quantum chemical study of a derivative of 3-substituted dithiocarbamic flavanone. Spectroc. Acta A **172**, 115–125 (2017)
45. Ibeji, C.U.; Adejoro, I.A.; Adeleke, B.B.: Quantum descriptors and corrosion inhibition potentials of amodaquine and nivaquine. J. Phys. Chem. Biophys. **5**, 1–11 (2015)
46. Ouakki, M.; Galai, M.; Rbaa, M.; Abousalem, A.S.; Lakhrissi, B.; Rifi, E.H.; Cherkaoui, M.: Quantum chemical and experimental evaluation of the inhibitory action of two imidazole derivatives on mild steel corrosion in sulphuric acid medium. Heliyon **5**, e02759 (2019)
47. El-Hajjaji, F.; Ech-chihbi, E.; Rezki, N.; Benhiba, F.; Taleb, M.; Chauhan, D.S.; Quraishi, M.A.: Electrochemical and theoretical insights on the adsorption and corrosion inhibition of novel pyridinium-derived ionic liquids for mild steel in 1 M HCl. J. Mol. Liq. **314**, 113737 (2020)
48. Abdulazeez, I.; Khaled, M.; Al-Saadi, A.A.: Impact of electron-withdrawing and electron-donating substituents on the corrosion inhibitive properties of benzimidazole derivatives: a quantum chemical study. J. Mol. Struct. **1196**, 348–355 (2019)
49. Ramya, K.; Mohan, R.; Anupama, K.K.; Joseph, A.: Electrochemical and theoretical studies on the synergistic interaction and corrosion inhibition of alkyl benzimidazoles and thiosemicarbazide pair on mild steel in hydrochloric acid. Mater. Chem. Phys. **149–150**, 632–647 (2015)
50. Rbaa, M.; Benhiba, F.; Obot, I.B.; Oudda, H.; Warad, I.; Lakhrissi, B.; Zarrouk, A.: Two new 8-hydroxyquinoline derivatives as an efficient corrosion inhibitor for mild steel in hydrochloric acid: synthesis, electrochemical, surface morphological, UV– visible and theoretical studies. J. Mol. Liq. **276**, 120–133 (2019)
51. Ghailane, T.; Balkhmima, R.A.; Ghailane, R.; Souizi, A.; Touir, R.; Ebn Touhami, M.; Marakchi, K.; Komiha, N.: Experimental and theoretical studies for mild steel corrosion inhibition in 1 M HCl by two new benzothiazine derivatives. Corros. Sci. **76**, 317–324 (2013)
52. ElAdnani, Z.; Mcharfi, M.; Sfaira, M.; Benzakour, M.; Benjelloun, A.T.; Ebn Touhami, M.: DFT theoretical study of 7-R-3methylquinoxalin-2(1H)-thiones (R@H; CH3; Cl) as corrosion inhibitors in hydrochloric acid. Corros. Sci. **68**, 223–230 (2013)
53. Vanasundari, K.; Balachandran, V.; Kavimani, M.; Narayana, B.: Spectroscopic investigation, vibrational assignments, Fukui functions, HOMO-LUMO, MEP and molecular docking evaluation of 4-[(3, 4-dichlorophenyl) amino] 2-methylidene 4-oxo butanoic acid by DFT method. J. Mol. Struct. **1147**, 136–147 (2017)
54. Obot, I.B.; Obi-Egbedi, N.; Ebenso, E.E.; Afolabi, A.; Oguzie, E.: Experimental, quantum chemical calculations, and molecular dynamic simulations insight into the corrosion inhibition properties of 2-(6-methylpyridin-2-yl)oxazolo[5,4- f][1,10]phenanthroline on mild steel. Res. Chem. Intermed. **39**, 1927–1948 (2013)
55. El Bakri, Y.; Guo, L.; Anouar, E.H.; Harmaoui, A.; Ben Ali, A.; Essassi, E.M.; Mague, J.T.: Synthesis, crystal structure, DFT, molecular dynamics simulation and evaluation of the anticorrosion performance of a new pyrazolotriazole derivative. J. Mol. Struct. **1176**, 290–297 (2018)
56. Kaya, S.; Guo, L.; Kaya, C.; Tüzün, B.; Obot, I.B.; Touir, R.; Islam, N.: Quantum chemical and molecular dynamic simulation studies for the prediction of inhibition efficiencies of some piperidine derivatives on the corrosion of iron. J. Taiwan Inst. Chem. Eng. **65**, 522–529 (2016)
57. Salarvand, Z.; Amirnasr, M.; Talebian, M.; Raeissi, K.; Meghdadi, S.: Enhanced corrosion resistance of mild steel in 1 M HCl solution by trace amount of 2-phenylbenzothiazole derivatives: experimental, quantum chemical calculations and molecular dynamics (MD) simulation studies. Corros. Sci. **114**, 133–145 (2017)